JACS
JOURNAL OF THE AMERICAN CHEMICAL SOCIETY
Article
pubs.acs.org/JACS

Systematic Study of Compositional and Synthetic Control of Vacancy and Magnetic Ordering in Oxygen-Deficient Perovskites $Ca_2Fe_{2-x}Mn_xO_{5+y}$ and $CaSrFe_{2-x}Mn_xO_{5+y}$ (x = 1/2, 2/3, and 1; y = 0−1/2)

Farshid Ramezanipour,[†] John E. Greedan,*[,†,‡] Lachlan M. D. Cranswick,[§] V. Ovidiu Garlea,[∥] Ronald L. Donaberger,[§] and Joan Siewenie[⊥]

[†]Department of Chemistry, McMaster University, Hamilton, Ontario, Canada, L8S 4M
[‡]Brockhouse Institute for Materials Research, McMaster University, Hamilton, Ontario, Canada, L8S 4M
[§]Canadian Neutron Beam Centre, National Research Council, Chalk River Laboratories, Chalk River, Ontario, Canada, K0J 1J0
[∥]Neutron Scattering Sciences Division, Oak Ridge National Laboratory, Oak Ridge, Tennessee 37831, United States
[⊥]Lujan Neutron Scattering Center, Los Alamos National Laboratory, Los Alamos, New Mexico 87545, United States

ABSTRACT: Ten compounds belonging to the series of oxygen-deficient perovskite oxides $Ca_2Fe_{2-x}Mn_xO_5$ and $CaSrFe_{2-x}Mn_xO_{5+y}$, where x = 1/2, 2/3, and 1 and $y \approx 0-0.5$, were synthesized and investigated with respect to the ordering of oxygen vacancies on both local and long-range length scales and the effect on crystal structure and magnetic properties. For the set with $y \approx 0$ the oxygen vacancies always order in the long-range sense to form the brownmillerite structure containing alternating layers of octahedrally and tetrahedrally coordinated cations. However, there is a change in symmetry from *Pnma* to *Icmm* upon substitution of Sr for one Ca for all x, indicating local T_d chain (vacancy) disorder. In the special case of $CaSrFeMnO_5$ the neutron diffraction peaks broaden, indicating only short-range structural order on a length scale of ∼160 Å. This reveals a systematic progression from Ca_2FeMnO_5 (*Pnma*, well-ordered tetrahedral chains) to $CaSrFeMnO_5$ (*Icmm*, disordered tetrahedral chains, overall short-range order) to Sr_2FeMnO_5 ($Pm\bar{3}m$, destruction of tetrahedral chains in a long-range sense). Systematic changes occur in the magnetic properties as well. While long-range antiferromagnetic order is preserved, the magnetic transition temperature, T_c, decreases for the same x when Sr substitutes for one Ca. A review of the changes in T_c for the series $Ca_2Fe_{2-x}M_xO_5$, taking into account the tetrahedral/octahedral site preferences for the various M^{3+} ions, leads to a partial understanding of the origin of magnetic order in these materials in terms of a layered antiferromagnetic model. While in all cases the preferred magnetic moment direction is (010) at low temperatures, there is a cross over for x = 0.5 to (100) with increasing temperature for both the $Ca_2Fe_{2-x}Mn_xO_5$ and the $CaSrFe_{2-x}Mn_xO_5$ series. For the $y > 0$ phases, while a brownmillerite ordering of oxygen vacancies is preserved for the Ca_2 phases, a disordered $Pm\bar{3}m$ cubic perovskite structure is always found when Sr is substituted for one Ca. Long-range magnetic order is also lost, giving way to spin glass or cluster-glass-like behavior below ∼50 K. For the x = 0.5 phase, neutron pair distribution function (NPDF) studies show a local structure related to brownmillerite ordering of oxygen vacancies. Neutron diffraction data at 3.8 K show a broad magnetic feature, incommensurate with any multiple of the chemical lattice, and with a correlation length (magnetic domain) of 6.7(4) Å.

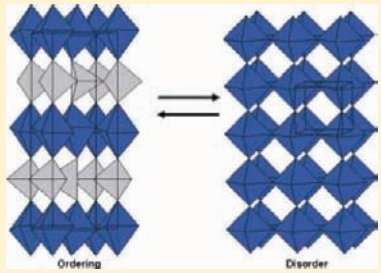

INTRODUCTION

The rich chemistry and versatile physical properties observed in oxygen-deficient perovskites have made them an attractive family of materials. They have been investigated as potential functional materials in areas such as multiferroicity,[1] colossal magnetoresistance,[2,3] and mixed-conducting membranes for oxygen permeation purposes.[4−6] Understanding the parameters that control the properties of this family of compounds is therefore of significant importance. This paper reports a systematic study of a family of oxygen-deficient perovskite materials with general composition $AA'B_{2-x}B_x'O_{5+y}$ with cation substitutions on both the A and the B sites along with the presence of a high concentration of vacancies on the oxygen site. Specifically, the cation choices are A = A′ = Ca and A = Ca, A′ = Sr, B = Fe and B′ = Mn with x = 0.5, 0.67, and 1.0 and $y \approx 0-0.5$ for a total of 10 new compounds, as one member of the series, $Ca_2FeMnO_{5.0}$, has recently been studied.[7] It is of considerable interest to determine the effect of the cation substitutions and the level of oxygen deficiency on the structure, both average and local, and on selected physical properties, in this case magnetic properties, of these phases in comparison with $Ca_2Fe_2O_5$, $Sr_2Fe_2O_{5+y}$, $Ca_2FeMnO_{5.0}$, Sr_2FeMnO_{5+y}, $Ca_2Fe_{1.5}Cr_{0.5}O_{5.0}$, and $Sr_2Fe_{1.5}Cr_{0.5}O_{5+y}$ which have been studied previously.[7−14]

Concerning the crystal structure, by far the most common structure type for perovskite compositions with $y \approx 0$ is that of brownmillerite. In this case the high concentration of nominal oxygen vacancies, 16. 67%, order in a long-range sense resulting in a supercell with dimensions $a_{bm} \approx c_{bm} \approx 2^{1/2}a_p$ and $b_{bm} \approx 4a_p$, where a_p is the primitive cubic perovskite cell edge, featuring

Received: November 22, 2011
Published: January 10, 2012

   dx.doi.org/10.1021/ja210985t | J. Am. Chem.Soc. 2012, 134, 3215−3227

alternating layers of octahedrally coordinated B ions and chains of tetrahedrally coordinated B′ ions. Each octahedron shares four corners with neighboring octahedra, and each tetrahedron shares two corners with the adjacent tetrahedra. The octahedral layers and tetrahedral chains are linked in three dimensions by the remaining sites. Note that the average cation coordination number is five.

Brownmillerites crystallize in a number of space groups *Ibm*2, *Pnma*, *Icmm*, *Pbcm*, and *C*2/*c*, which are determined by the relative orientations of the tetrahedral chains between layers and in case of *Pbcm* and *C*2/*c*, also within the layers. The relationship between space group symmetry and relative chain orientations has been discussed by several authors, and the details will not be repeated here.[15,16] It is possible, however, to devise a hierarchy of symmetries in terms of the constraints on the chain ordering from greatest to least as follows

$$Pbcm > Pnma, Ibm2 > Icmm > Pm\bar{3}m$$

for which primitive cubic symmetry is included where the tetrahedral chains are completely destroyed in the long-range sense. In *Icmm* the chains still exist, but the orientations are disordered both within and between layers.

Attempts have been made to correlate the observed space groups with structural parameters. One recent scheme uses the interlayer separation between the chains versus the angle of distortion from 180° within the chains, and with the exception of one case, Ca_2FeCoO_5, an excellent correlation results.[15,16] In terms of the materials studied here, the effect of an increase in the A-site cation radius increases the interlayer chain separation, and the phase diagram of ref 15 predicts the space group sequence *Pnma* to *Ibm*2 to *Icmm*. For example $Ca_2Fe_2O_5$ crystallizes in *Pnma*, while $Sr_2Fe_2O_5$ occurs in *Icmm*.[8,10] It is of interest to determine the result for the series where Sr replaces one Ca. Continuing with phases with $y \approx 0$, there are at least two examples of reported $Pm\bar{3}m$ symmetry: $Sr_2Fe_{1.5}Cr_{0.5}O_{5+y}$ with $y \approx 0.11$[14] and Sr_2FeMnO_{5+y} with $y \approx 0$.[12] In the latter case, there is evidence that the local structure, as determined from neutron pair distribution function studies, can be described for short r (to ~5 Å) in terms of a brownmillerite model. As the Ca analogs of the above phases, $Ca_2Fe_{1.5}Cr_{0.5}O_5$ and Ca_2FeMnO_5, are both brownmillerites, the results for AA′ = CaSr are of keen interest.

In the case of $y \approx 0.5$ there is scant evidence for the existence of such phases for the AA′ = Ca_2 series members, although systematic studies appear not to have been done.

For the case of Ca_2FeMnO_{5+y} two results are on record with different unit cell volumes but the same space group symmetry, *Pnma*.[7,17] Reference 17 reports a room-temperature cell volume of 436.7 Å^3, while a volume of 443.7 Å^3 is listed in ref 7.

A value of $y \approx 0.2$ has been estimated for the more oxidized phase. In contrast, for AA′ = Sr_2 long-range vacancy ordered phases exist for $y \geq 0.5$, notably, $Sr_2Fe_2O_{5.5}$ (often reported as $Sr_4Fe_4O_{11}$), which crystallizes in *Cmmm* with supercell, $a \approx 2 \times 2^{1/2}a_p$, $b \approx 2a_p$, $c \approx 2^{1/2}a_p$,[11] and $Sr_2Fe_2O_{5.75}$ ($Sr_8Fe_8O_{23}$) *I*4/*mmm* with supercell, $a \approx 2 \times 2^{1/2}a_p$, $c \approx 2\ a_p$. However, $Pm\bar{3}m$ examples are reported as well, $Sr_2Fe_{1.5}Cr_{0.5}O_{5+y}$ with $y \approx 0.39-0.53$ and $Sr_2FeMnO_{5.5}$.[12,14] Again, the results for the AA′ = CaSr members should be illuminating.

For phases showing brownmillerite vacancy ordering, long-range magnetic order is always found. Magnetic structural studies always find a so-called G-type antiferromagnetic order with rather high critical temperatures, T_c, ranging from 730(2) ($Ca_2Fe_2O_5$)[18] to 407(2) K (Ca_2FeMnO_5).[7] A systematic analysis of the dependence of T_c on the composition of the BB′ sites does not apparently exist. For example, some B-site substitutions are highly site specific. Ga is known to favor the T_d site,[19,20] while Mn[7] and Cr[13] have a strong O_h site preference. An initial effort to understand the systematics of T_c will be presented here. In addition, two distinct magnetic anisotropies are found: G_x where the moment direction is along the shortest axis, usually *a*, and G_y where the moment preference is for the longest axis, usually the *b* axis. $Ca_2Fe_2O_5$ has G_x, while Ca_2FeMnO_5 and Ca_2GaMnO_5 show G_y. It is of interest to determine the crossover composition for the $Fe_{2-x}Mn_x$ series.

In the case of $Pm\bar{3}m$ phases, long-range magnetic ordering is usually quenched.

Sr_2FeMnO_{5+y} with $y \approx 0$ and 0.5 shows only short-range magnetic order, although there is evidence from Mössbauer data that some $Sr_2Fe_{1.5}Cr_{0.5}O_{5+y}$ compositions are long-range ordered.[14] The situation for the AA′ = CaSr series members is unknown.

EXPERIMENTAL SECTION

Synthesis. The pellets made from stoichiometric amounts of $CaCO_3$ (99.99% Alfa Aesar), $SrCO_3$ (99.9% Sigma Aldrich), Fe_2O_3 (99.998% Alfa Aesar), and Mn_2O_3 (99.9% Cerac) were fired at 1250 °C in an argon atmosphere to give phases with $y \approx 0$. The syntheses were also repeated in air to obtain phases with higher oxygen content $y \approx 0.5$. The heating and cooling rates were both ~100 °C/h. Several intermediate grindings and refirings were performed. For the brownmillerite $CaSrFeMnO_5$ phase, synthesis was repeated multiple times at temperatures as high as 1350 °C to examine the effect of temperature on the crystallinity; however, no significant changes were observed.

Thermal Gravimetric Analysis (TGA). A Netzsch STA-409 TGA-DTA Instruments (thermal gravimetric analyzer-differential thermal analyzer) was used to measure the weight losses of the vacancy-disordered air-synthesized $CaSrFe_{2-x}Mn_xO_{5+y}$ samples upon losing oxygen in an argon atmosphere at 1250 °C to be converted to the vacancy-ordered brownmillerites for which $y \approx 0$ is assumed.

X-ray and Neutron Diffraction. Powder X-ray data were obtained on a PANalytical X'Pert Pro MPD diffractometer with a linear X'Celerator detector with a 2θ step interval of 0.0084° using Cu Kα_1 radiation (λ = 1.54056 Å).

Powder neutron data with fixed wavelengths were acquired on the C2 diffractometer at the Canadian Neutron Beam Centre at Chalk River, Ontario, and the HB2A diffractometer, at the High Flux Isotope Reactor at the Oak Ridge National Lab. Time of flight neutron diffraction data were obtained on the instrument NPDF[21] at the M. Lujan Jr. Center for Neutron Scattering at the Los Alamos Neutron Science Center.

Bulk Magnetic Measurements. Magnetic susceptibility data versus temperature as well as magnetization versus field data were obtained on a Quantum Design MPMS SQUID Magnetometer. Gelatin capsules were used as sample holders for the temperature range 5−300 K and quartz tubes for 320−700 K.

RESULTS AND DISCUSSION

Crystal Structures of the $Ca_2Fe_{2-x}Mn_xO_{5+y}$, $y \approx 0$ Series, Synthesized in Argon. The results of crystal structure refinements for x = 0.50 and 0.67 at 300 K are shown in Tables 1 and 2. As expected, the space group is *Pnma* and the Mn ions prefer the octahedral site. In the initial stages the tetrahedral site occupations were refined but the result gave 100% occupation by Fe to within error. The refined Fe/Mn octahedral site occupancies are in good agreement, within a few percent, with the nominal compositions. A plot of the unit cell volume for the solid solution $Ca_2Fe_{2-x}Mn_xO_{5.0}$ up to x = 1.0 is shown in Figure 1a, indicating adherence to Vegard's Law.

dx.doi.org/10.1021/ja210985t | J. Am. Chem.Soc. 2012, 134, 3215−3227

Table 1. Cell Constants, Agreement Indices, Atomic Positions, and Displacement Factors at 300 K for $Ca_2Fe_{2-x}Mn_xO_{5.0}$, x = 0.50 and 0.67 (Synthesized in Argon)

		x = 0.50		x = 0.67	
space group		*Pnma* (No. 62)		*Pnma* (No. 62)	
a (Å)		5.36219(21)		5.33845(22)	
b (Å)		15.0508(6)		15.1540(6)	
c (Å)		5.52838(22)		5.50085(23)	
V (Å^3)		446.17(5)		445.01(5)	
R_{wp}		0.0412		0.0437	
GOF		1.78		1.74	
	x	y	z	U_{iso}	Occ.
$Ca_2Fe_{1.5}Mn_{0.5}O_{5.0}$					
Ca	−0.0168(9)	0.10930(21)	0.4772(7)	0.0123(11)	1.0
Fe1	0.9467(5)	0.25	0.9375(5)	0.0078(8)	1.0
Mn	0.0	0.0	0.0	0.0070(26)	0.486(4)
Fe2	0.0	0.0	0.0	0.0070(26)	0.514(4)
O1	0.2652(8)	−0.01449(18)	0.2371(6)	0.0076(8)	1.0
O2	0.0240(7)	0.14121(18)	0.0689(5)	0.0124(9)	1.0
O3	0.0959(8)	0.25	−0.3796(8)	0.0107(14)	1.0
$Ca_2Fe_{1.33}Mn_{0.67}O_{5.0}$					
Ca	−0.0138(9)	0.10961(20)	0.4789(6)	0.0105(13)	1.0
Fe1	0.9463(5)	0.25	0.9369(5)	0.0082(11)	1.0
Mn	0.0	0.0	0.0	0.013(9)	0.637(4)
Fe2	0.0	0.0	0.0	0.013(9)	0.363(4)
O1	0.2632(9)	−0.01357(18)	0.2387(7)	0.0113(11)	1.0
O2	0.0242(7)	0.14127(18)	0.0678(5)	0.0126(11)	1.0
O3	0.0938(8)	0.25	−0.3807(8)	0.0118(16)	1.0

Table 2. Selected Interatomic Distances (Å) and Angles (Deg) at 300 K for $Ca_2Fe_{2-x}Mn_xO_{5.0}$ (Synthesized in Argon)

bond or angle	x = 0.50	x = 0.67
Fe1−O2	1.839(3) × 2	1.846(3) × 2
Fe1−O3	1.908(5)	1.907(5)
Fe1−O3	1.927(5)	1.916(5)
Mn(Fe2)−O1	1.936(4) × 2	1.925(4) × 2
Mn(Fe2)−O1	1.946(4) × 2	1.934(4) × 2
Mn(Fe2)−O2	2.163(3) × 2	2.177(3) × 2
Ca−O1	2.433(6)	2.439(6)
Ca−O1	2.498(5)	2.511(5)
Ca−O1	2.511(5)	2.517(5)
Ca−O1	2.742(5)	2.723(5)
Ca−O2	2.318(4)	2.321(4)
Ca−O2	2.522(5)	2.526(5)
Ca−O2	2.950(5)	2.923(5)
Ca−O3	2.340(4) × 2	2.335(4) × 2
Fe1−O3−Fe1	124.2(2)	123.6(3)
Fe1−O2−Mn(Fe2)	142.4(2)	142.9(2)
Mn(Fe2)−O1−Mn(Fe2)	165.6(2)	166.5(2)

Note the inverse correlation with the b-axis length, Figure 1b. This results from the fact that the Jahn−Teller ion, Mn^{3+}, substitutes selectively on the octahedral site. The distances between the tetrahedral layers and the tetrahedral chain distortion angles that were used to construct the structure field map for brownmillerites in ref 15 were also measured. The tetrahedral layer distances are 7.5254 and 7.5770 Å for x = 0.5 and 0.7, respectively. Also, the distortion angles for the tetrahedral chains are 56.25° and 56.62° for x = 0.5 and 0.7, respectively. These values are consistent with the proposed structure map[15] and place both of the $Ca_2Fe_{2-x}Mn_xO_5$ compounds in the *Pnma* region of that map.

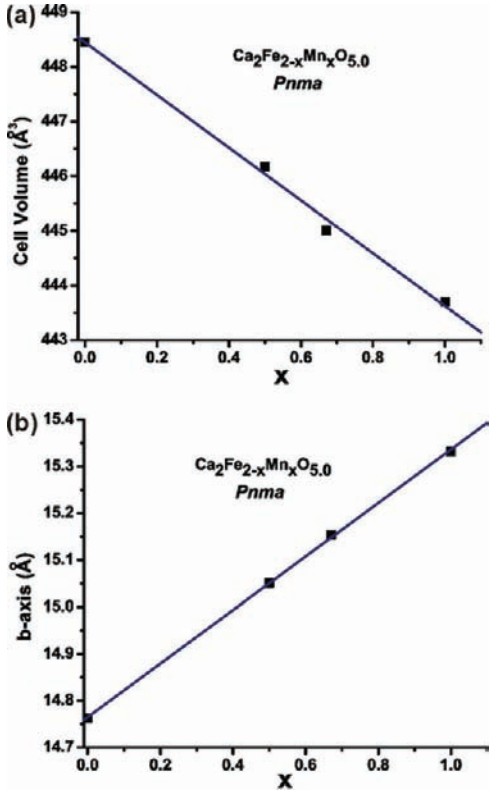

Figure 1. (a) Vegard's law correlation between the unit cell volume and x for $Ca_2Fe_{2-x}Mn_xO_{5.0}$ (synthesized in argon). (b) Correlation between the b-axis length and x.

dx.doi.org/10.1021/ja210985t | J. Am. Chem.Soc. 2012, 134, 3215−3227

Table 3. Unit Cell Constants and Agreement Indices for $CaSrFe_{2-x}Mn_xO_{5.0}$, x = 0.50 and 0.67, Synthesized in Argon, and Atomic Positions, Displacement Factors, and Site Occupancies at 300 K in *Icmm*[a]

			x = 0.50		x = 0.67	
space group			*Icmm* (No. 74)		*Icmm* (No. 74)	
a (Å)			5.5630(3)		5.5344(4)	
b (Å)			15.4625(8)		15.5129(12)	
c (Å)			5.4172(3)		5.4093(4)	
V (Å^3)			465.97(6)		464.41(9)	
R_{wp}			0.0454		0.0461	
GOF			2.65		2.27	
	x	y	z	U_{iso}	Occ.	site multiplicity
$CaSrFe_{1.5}Mn_{0.5}O_{5.0}$						
Ca/Sr	0.5165(7)	0.6103(2)	0.0	0.0146(11)	1.0	8
Fe1	0.5675(6)	0.25	0.4485(7)	0.006(1)	0.489(3)	8
Mn1	0.5675(6)	0.25	0.4485(7)	0.006(1)	0.011(3)	8
Mn2	0.0	0.0	0.0	0.016(3)	0.459(5)	4
Fe2	0.0	0.0	0.0	0.016(3)	0.541(5)	4
O1	0.25	0.9920(2)	0.25	0.014(1)	1.0	8
O2	0.0548(7)	0.1413(2)	0.0	0.020(1)	1.0	8
O3	0.625(1)	0.25	0.107(1)	0.021(2)	0.5	8
$CaSrFe_{1.33}Mn_{0.67}O_{5.0}$						
Ca/Sr	0.5151(8)	0.6124(2)	0.0	0.016(1)	1.0	8
Fe1	0.5642(8)	0.25	0.451(1)	0.011(2)	0.464(4)	8
Mn1	0.5642(8)	0.25	0.451(1)	0.011(2)	0.036(4)	8
Mn2	0.0	0.0	0.0	0.020(5)	0.561(7)	4
Fe2	0.0	0.0	0.0	0.020(5)	0.439(7)	4
O1	0.25	0.9918(3)	0.25	0.015(1)	1.0	8
O2	0.0481(9)	0.1398(3)	0.0	0.023(1)	1.0	8
O3	0.628(2)	0.25	0.114(2)	0.036(3)	0.5	8

[a]The refined Fe and Mn contents are very close to the stoichiometric values.

Crystal Structures of the $CaSrFe_{2-x}Mn_xO_{5+y}$, $y \approx 0$ Series, Synthesized in Argon. The results of crystal structure refinements for x = 0.50 and 0.67 at 300 K are shown in Tables 3 and 4. That for x = 1.0 will be discussed separately. For this series, the absence of the (131) reflection indicated I-centering. The data were refined in both *Ibm*2 and *Icmm* with the latter giving consistently lower R_{wp} and GOF values. For x = 0.5, the *Ibm*2 refinements give R_{wp} = 0.0589 and GOF=3.44, compared to R_{wp} = 0.0454 and GOF=2.65 for *Icmm*. Also, for x = 0.67, the *Ibm*2 agreement factors are R_{wp} = 0.0522 and GOF=2.56, as compared to R_{wp} = 0.0461 and GOF=2.27 for *Icmm*. As there are actually four fewer positional parameters for the *Icmm* setting, these results are taken as a strong argument for choosing this space group. As for the AA′ = Ca_2 series, site occupations were refined in the initial stages. The Ca/Sr ratio always refined to 1.0 to within the estimated error. However, unlike for the AA′ = Ca_2 materials, there was clear evidence for some Fe/Mn mixing on the T_d sites ranging from 2% to 7% as indicated in Table 3. Nevertheless, note that this apparent site mixing is still small and possibly near the limit of detection using Rietveld methods. The same trends are seen with respect to changes in cell volume and b-axis length with increased Mn content as for the AA′ = Ca_2 series. Comparing the cell volumes, interatomic distances, and angles between the AA′ = Ca_2 and CaSr series for the same x one notes the expected increases in cell volume of ∼4% due to the larger radius of Sr^{2+}, increases in the b-axis length (2−3%), increases in the axial Mn(Fe2)−O bond lengths, an increase in the interplanar Mn(Fe2)−O−Mn(Fe2) angle of about 7°, and a similar increase in the Fe1−O−Mn(Fe2) angle which connects the T_d chains to the O_h layers. However, the *Icmm* space group for the CaSr phases is not consistent with the structure map proposed in ref 15. The tetrahedral chain separations (7.7313 and 7.7565 Å for x = 0.5 and 0.67, respectively) and tetrahedral chain distortion angles (54.36° and 53.18° for x = 0.5 and 0.67, respectively) would put $CaSrFe_{2-x}Mn_xO_5$ in the *Ibm*2 region of that map.

Table 4. Selected Interatomic Distances (Å) and Angles (Deg) for $CaSrFe_{2-x}Mn_xO_{5.0}$ at 300 K

bond or angle	x = 0.50	x = 0.67
Fe1−O2	1.834(3) × 2	1.838(4) × 2
Fe1−O3[a]	1.878(7), 1.911(6)	1.855(11), 1.921(9)
Fe1−O3[a]	1.733(7), 2.430(8)	1.741(9), 2.379(11)
Mn(Fe2)−O1	1.9451(2) × 4	1.9389(3) × 4
Mn(Fe2)−O2	2.206(3) × 2	2.185(4) × 2
Ca/Sr−O1	2.556(3) × 2	2.568(4) × 2
Ca/Sr−O1	2.620(4) × 2	2.650(4) × 2
Ca/Sr−O2	2.7592(8) × 2	2.7439(9) × 2
Ca/Sr−O2	3.214(5)	3.146(6)
Ca/Sr−O3	2.373(4)	2.358(5)
Fe1−O3−Fe1	126.6(4)	128.3(5)
Mn(Fe2)−O1−Mn(Fe2)	172.7(2)	172.5(3)

[a]The inherent disorder in this space group (both Fe1 and O3 have an occupation of 0.5) renders difficult assignment of bond lengths to the Fe1−O3 part of the polyhedron.

Remarkably, the situation for x = 1.0 is quite different. From observation of the neutron powder diffraction pattern for this phase it was clear that all of the diffraction peaks were significantly broader relative to the x = 0.5 and 0.67 series members. This is seen in Figure 2, where the long-wavelength, low-angle part of the

dx.doi.org/10.1021/ja210985t | J. Am. Chem.Soc. 2012, 134, 3215−3227

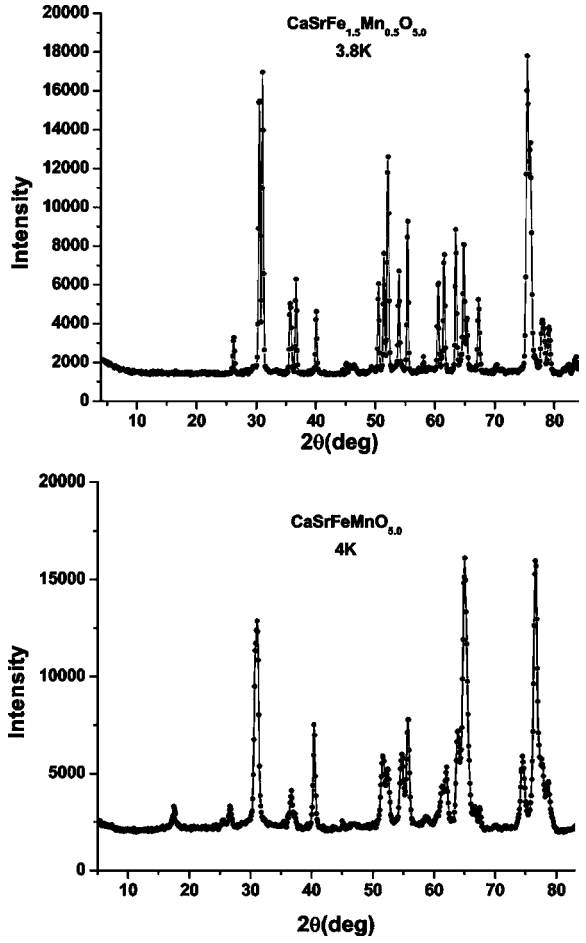

Figure 2. Comparison of the neutron diffraction patterns (λ = 2.37 Å) for $CaSrFe_{1.5}Mn_{0.5}O_{5.0}$ (top) and $CaSrFeMnO_{5.0}$ (bottom). Note the clear broadening of the reflections for the latter.

pattern is compared for the x = 1.0 and 0.5 materials. The pattern for x = 1.0 can be fitted to the *Icmm* model as for x = 0.50 and 0.67. An effort was made to estimate the "domain size" for the *Icmm* phase. This consisted of an analysis of the (121) reflection, near 40° in 2θ, which is not overlapped by any adjacent reflections. Fits of this peak for both x = 1.0 and 0.67 were carried out with both a Gaussian and a Lorentzian model. For x = 0.67 the Gaussian fit was excellent, yielding fwhm = 0.215(5)° and R = 0.997, while for x = 1.0 the Gaussian fit was poorer, R = 0.989 and the fwhm =0.34(1)°. The data were converted to Q for the Lorentzian fits to the function $I(Q) = A/((Q_0 - Q)^2 - \kappa^2)$,[22] where κ is the inverse correlation length or domain size and Q_0 is the peak position. In this case the inverse was true: the Lorentzian function fitted much better in the x = 1.0 case, while the fit was obviously poorer for x = 0.67. The fit of the x = 0.67 data yielded a resolution-limited κ_{res} = 0.0051(3) Å^{-1}, while κ for x = 1.0 was 0.0079(3) Å^{-1}. Finally, the domain size was estimated from $\xi = 1/(\kappa^2 - \kappa_{res}^2)^{1/2}$ = 166(12) Å.

This observation concerning the $CaSrFeMnO_{5.0}$ phase is remarkable but consistent with the trend $Ca_2FeMnO_{5.0}$ (*Pnma* brownmillerite)[7] → $CaSrFeMnO_{5.0}$ (short range, ~160 Å, *Icmm* brownmillerite domains) → $Sr_2FeMnO_{5.0}$ ($Pm\bar{3}m$ defect perovskite, at most local (~5 Å) brownmillerite domains),[12] that is, for this Fe/Mn ratio and for the same preparation conditions, in argon atmosphere, as the average radius of the AA′ site cations is systematically increased the degree of local T_d chain(vacancy) ordering is diminished and finally the chains themselves are destroyed, i.e., the vacancies are random in the long-range sense.

DC Susceptibility for $Ca_2Fe_{2-x}Mn_xO_{5.0}$ ($y \approx 0$ Series) Synthesized in Argon. As reported previously for the x = 1.0 phase, the bulk susceptibility below 300 K for both x = 0.50 and 0.67 showed no evidence for paramagnetic behavior. The high-temperature data, 300−700 K, were examined in an effort to locate T_c, which is expected to lie between 730 ($Ca_2Fe_2O_5$)[18] and 407 K (Ca_2FeMnO_5).[7] As will be discussed later, these data were not definitive. Examples for x = 0.50 and 0.67 are shown in Figure 3. Note anomalies near ~500 K for x = 0.50 and

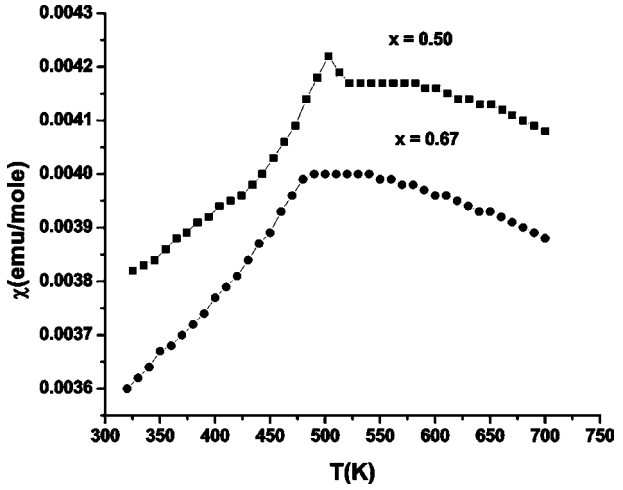

Figure 3. High-temperature susceptibility data for $Ca_2Fe_{2-x}Mn_xO_{5.0}$, x = 0.50 (top) and x = 0.67 (bottom).

~475 K for x = 0.67. Note that there is no evidence for paramagnetic behavior above these temperatures and out to 700 K. The presence of broad maxima is suggestive of short-range spin correlations.

DC Susceptibility for $CaSrFe_{2-x}Mn_xO_{5.0}$ ($y \approx 0$ Series) Synthesized in Argon. Comparable data are shown in Figure 4

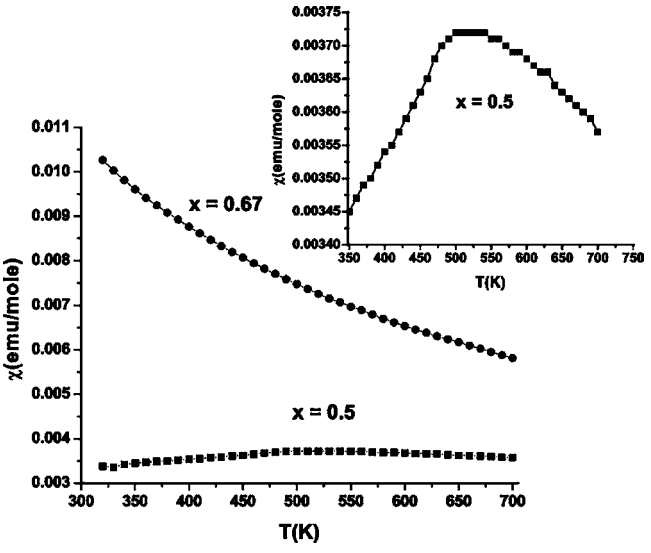

Figure 4. High-temperature susceptibility data for $CaSrFe_{2-x}Mn_xO_{5.0}$, x = 0.67 (top) and x = 0.50 (bottom). Data for x = 0.5 are shown separately in the inset, indicating a broad maximum near ~525 K.

dx.doi.org/10.1021/ja210985t | J. Am. Chem.Soc. 2012, 134, 3215−3227

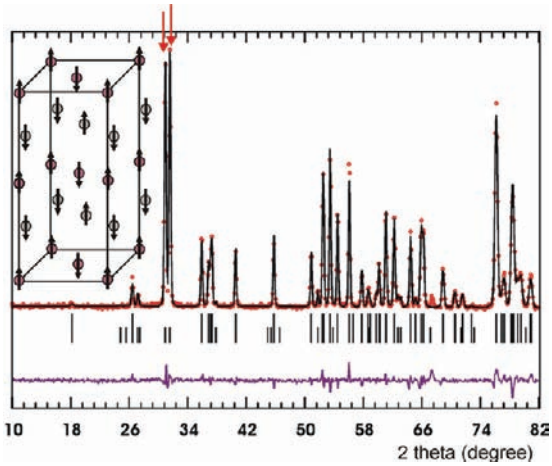

Figure 5. Refinement of the crystal and magnetic structures for $Ca_2Fe_{1.5}Mn_{0.5}O_{5.0}$ at 3.8 K. The unindexed peak at ~67.5° belongs to the vanadium sample holder. (Inset) Resulting G_y magnetic structure. Agreement indices and moment values for x = 0.5 and 0.67 phases for both series AA = Ca_2 and CaSr are included in Table 5.

Table 5. Summary of the Refinements of the Magnetic Structure, Estimated T_c, Agreement Indices, and Moment Values up to Room Temperature for $Ca_2Fe_{2-x}Mn_xO_{5.0}$ and $CaSrFe_{2-x}Mn_xO_{5.0}$

	estimated T_c, K	O_h site moment	T_d site moment	$R_{Magnetic}$
$Ca_2Fe_{1.5}Mn_{0.5}O_5$	465(2)			
4 K		3.94(8)	3.97(9)	1.02
50 K		3.93(8)	3.93(9)	1.53
100 K		3.86(8)	3.88(9)	1.75
150 K		3.76(9)	3.78(10)	1.56
300 K		3.1 (1)	3.2(1)	2.03
$Ca_2Fe_{1.33}Mn_{0.67}O_5$	423(2)			
4 K		3.97(8)	3.80(9)	1.65
50 K		3.89(9)	3.85(10)	2.05
100 K		3.8(1)	3.9(1)	2.00
150 K		3.7(1)	3.8(1)	2.46
175 K		3.5(1)	3.7(1)	2.94
200 K		3.5(1)	3.7(1)	1.60
225 K		3.4(1)	3.5(1)	2.49
250 K		3.2(1)	3.4(1)	2.52
275 K		3.1(1)	3.2(1)	3.08
300 K		2.9(1)	3.1(1)	2.81
$CaSrFe_{1.5}Mn_{0.5}O_5$	432(2)			
4 K		4.2(2)	4.0(2)	7.51
50 K		4.0(2)	4.0(2)	8.26
150 K		3.8(2)	3.9(2)	7.55
200 K		3.5(2)	3.8(2)	5.80
250 K		3.2(2)	3.6(2)	6.31
300 K		2.9(2)	3.3(2)	6.06
$CaSrFe_{1.33}Mn_{0.67}O_5$	403(2)			
4 K		3.7(2)	3.5(2)	8.23
50 K		3.6(1)	3.6(2)	7.45
100 K		3.6(2)	3.4(2)	9.58
150 K		3.4(2)	3.4(2)	8.13
175 K		3.4(2)	3.2(2)	7.31
200 K		3.2(2)	3.1(2)	8.04
225 K		3.2(2)	3.0(2)	7.34
250 K		3.0(2)	2.9(2)	7.63
275 K		2.8(3)	2.8(3)	7.76
300 K		2.6(2)	2.5(3)	11.0

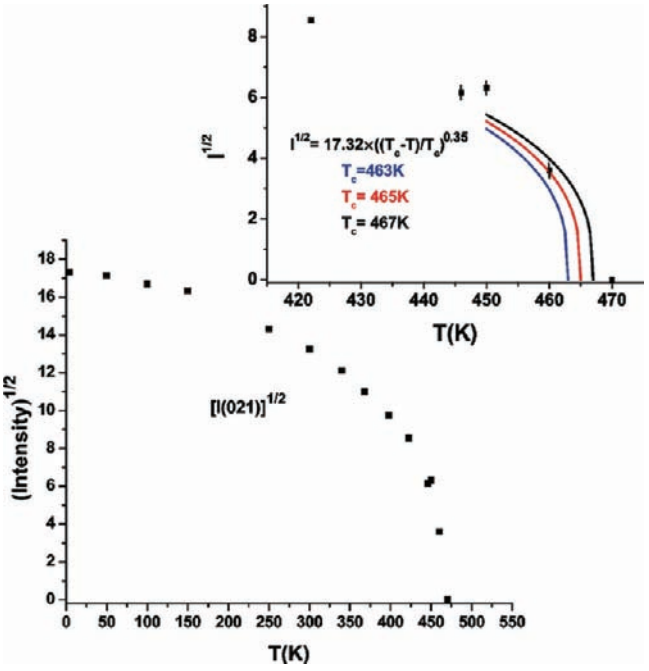

Figure 6. Estimation of T_c for $Ca_2Fe_{1.5}Mn_{0.5}O_5$ by plotting $[I(021)]^{1/2}$ versus T. Error bars are roughly the same size as the symbols. The method of estimating T_c, described in the text, is shown in the inset.

for the x = 0.5 and 0.67 members of the $CaSrFe_{2-x}Mn_xO_{5.0}$ series. For the x = 0.67 material no maximum is seen, while for x = 0.5 there is a broad maximum near 525 K. Attempts to fit the x = 0.67 data to a Curie–Weiss law yielded nonphysical parameters. As with the data for AA′ = Ca_2, there are no clear indications of a T_c for either composition.

Neutron Diffraction for AA′ = Ca_2 and CaSr Synthesized in Argon. Guided by experience with $Ca_2FeMnO_{5.0}$, neutron diffraction data were obtained at several temperatures and analyzed to determine the magnetic structures and obtain a reliable estimate of T_c. The Rietveld refinement profile for x = 0.50, as representative of both the AA′ = Ca_2 and the AA′ = CaSr series, is shown in Figure 5, which involves a joint refinement of the magnetic and crystal structure. The more intense magnetic reflections are marked with arrows. The two strongest near 31° can be indexed as (021) and (120) as found for the x = 1.0 phase[7] and are indicative of a G_y magnetic structure shown in the inset to Figure 5. As indicated, the preferred moment direction (at 3.8 K) is along the b axis (longest axis). The refined magnetic moments and agreement indices for each temperature for the x = 0.5 and 0.67 members of both the AA′ = Ca_2 and the AA′ = CaSr series are given in Table 5. As noted previously for Ca_2FeCoO_5, the ratio of the intensities of the two major magnetic reflections, $I(021)/I(120)$, is determined by the preferred moment direction.[16] A ratio ~1.0 indicates G_y, while one near ~3.0 indicates G_x where the moments are aligned along the shortest axis.

In order to estimate T_c the intensity of the (021) reflection versus temperature is plotted in Figure 6 and is seen to vanish near 465 K. More precise estimates of T_c can be obtained by fitting data obtained in the critical regime, very close to T_c, to a function such as $I^{1/2} = I_{sat}{}^{1/2}((T_c - T)/T_c)^{\beta}$, where I_{sat} is the intensity at the lowest temperature and β is the critical exponent. Unfortunately, for nearly all samples there were perhaps only one or two data points within the critical regime. Thus, T_c was estimated by comparison of plots of $I^{1/2}$ versus T with those generated taking different choices for T_c. A β value

dx.doi.org/10.1021/ja210985t | J. Am. Chem.Soc. 2012, 134, 3215–3227

of 0.35 was taken; it is roughly an average for three-dimensional Ising, XY, and Heisenberg models.[23] A typical plot is shown in the inset to Figure 6. The estimated error for determination of T_c is ±2 to ±3 K in most cases. T_c values determined in this manner are included in Table 5. For $Ca_2Fe_{1.5}Mn_{0.5}O_{5.0}$, T_c = 465(2) K, which is well below the peak near 500 K in the high-temperature susceptibility, Figure 3. The same is true for x = 0.67, where T_c = 423(2) K, whereas the susceptibility anomaly lies at ~475 K.

A change in magnetic anisotropy was noticed for $Ca_2Fe_{1.5}Mn_{0.5}O_{5.0}$ as the temperature increased to near T_c, as demonstrated in Figure 7. There is a clear cross over from G_y to

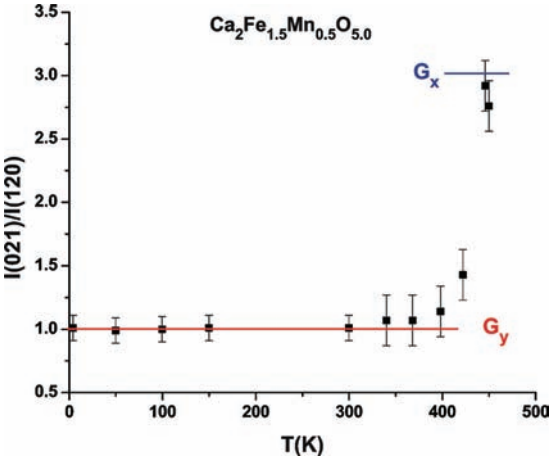

Figure 7. Ratio of the (021)/(120) magnetic reflections versus temperature for $Ca_2Fe_{1.5}Mn_{0.5}O_{5.0}$ showing a cross over from G_y to G_x beginning above 400 K. T_c for this compound is 465(2) K.

G_x beginning above 400 K. As the x = 0.0 member ($Ca_2Fe_2O_5$) is G_x and Ca_2FeMnO_5 is G_y, such a cross over might be anticipated but was not detected for the x = 1.0 and 0.67 phases. Repeating the neutron diffraction experiment on the same sample showed that the reorientation of magnetic anisotropy is reversible. A similar cross over was reported for Ca_2FeCoO_5, but in this case the onset occurred at 100 K and was complete by 200 K.[16]

In Figure 8 a summary of the known magnetic anisotropies in the AA′ = Ca_2 brownmillerite materials is presented. It seems

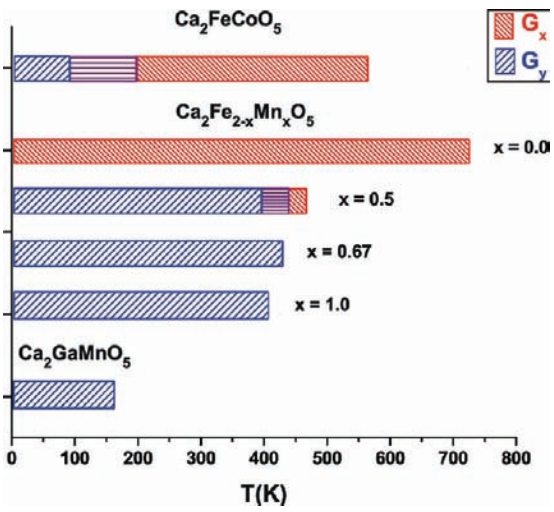

Figure 8. Summary of the known magnetic anisotropies for $Ca_2BB'O_5$ brownmillerites. G_x and G_y indicate the preferred orientation along the shortest and longest unit cell axes, respectively.

clear that Mn^{3+} strongly prefers the b (long) axis as does Co^{3+} but to a lesser degree, while Fe^{3+} prefers the a (shortest) axis. In these compounds, Mn^{3+} occupies the O_h sites nearly exclusively while Fe^{3+} is mainly on the T_d site when combined with Mn^{3+}. The situation is more complex for Ca_2FeCoO_5 as Fe^{3+} and Co^{3+} occupy both O_h and T_d sites.

In general, the trends shown by the $CaSrFe_{2-x}Mn_xO_{5.0}$ series are similar. The x = 0.50 and 0.67 phases also show a G_y magnetic structure, and there is indeed a cross over to G_x for x = 0.5 beginning at ~375 K which is complete by 410 K.

The final topic in this section is an attempt to rationalize the variation of T_c as a function of various cation substitutions on the BB′ sites for the family of $Ca_2Fe_{2-x}M_xO_{5.0}$ brownmillerites, where M^{3+} = Al, Ga, Mn, Cr, Sc, and Co. This information is presented in Figure 9. First, of course, one expects that any

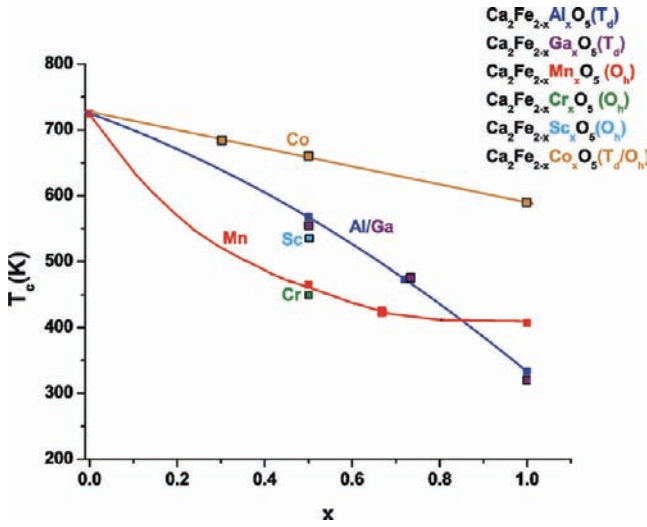

Figure 9. Variation of T_c for the family of $Ca_2Fe_{2-x}M_xO_{5.0}$ brownmillerites. Site preference for each M ion is indicated.

substitution for Fe^{3+}, which is an S = 5/2 ion, will result in a lowering of T_c. Among the different M cations there are two basic types: (1) diamagnetic ions which substitute primarily on the T_d sites, such as Al^{3+} and Ga^{3+},[19,20,24] and (2) magnetic ions which substitute on the O_h site, such as Mn^{3+}(S = 2)[7] and Cr^{3+} (S = 3/2).[25] In addition, Co^{3+} (S = 3/2, assuming high spin) substitutes equally on both sites,[16,20] and diamagnetic Sc^{3+} prefers the O_h site.[19,20] Several trends are worthy of note. First, for cations of type 1, the rate of decrease is relatively gradual out to x = 1.0, being well described by a convex polynomial curve. On the other hand, the decrease for type 2 ions is concave and quite pronounced for small x before leveling off beyond x = 0.5. Remarkably, substitution of diamagnetic Sc^{3+} at the O_h site results in a much higher T_c at x = 0.5 than magnetic Mn^{3+} or Cr^{3+}. At the end point x = 1.0 the order for T_c is M = $Co^{3+} \gg Mn^{3+} > Al^{3+}, Ga^{3+}$.

It is possible to understand some of these trends in terms of a layered antiferromagnetic (AF) model. This approach is supported by observation of broad susceptibility maxima above T_c for many of the compounds studied. Recall that brownmillerites consist of stacked layers of corner-sharing octahedra (CSO) and corner-sharing tetrahedra (CST). Within the CSO layers the superexchange Fe−O−M angle is large (~165° or so), and one expects strong 2D AF coupling when only Fe^{3+} occupies these sites. Within the CST layers the tetrahedra are linked only

dx.doi.org/10.1021/ja210985t | J. Am. Chem.Soc. 2012, 134, 3215−3227

in one dimension to each other but are shared by adjacent octahedral layers. The Fe−O−M superexchange angles are much more acute, and both weaker intrachain and interchain AF coupling is expected relative to that within the CSO layers. This situation is represented in Figure 10.

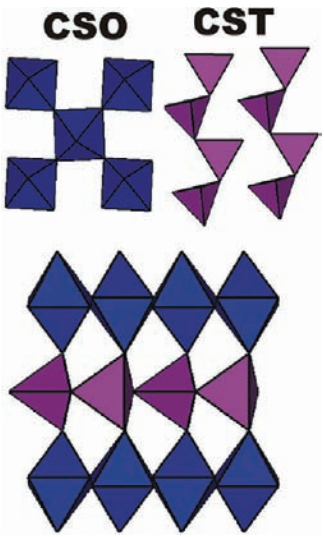

Figure 10. View of the corner-sharing octahedral layers (CSO) and corner-sharing tetrahedral layers (CST) and the linkage between the two for brownmillerites.

For layered AF materials the following relationship has been proposed[26]

$$k_B T_c \approx \xi^2_{2D} J_{inter} S^2 \quad (1)$$

where T_c is the critical temperature for 3D ordering, ξ^2_{2D} is the intralayer spin−spin correlation length, J_{inter} is the interlayer exchange, and S is the spin quantum number. For this analysis S^2 is replaced by $\langle S^2 \rangle$, the compositional average value. While eq 1 is strictly appropriate for systems with very weak J_{inter}, which is probably not the case here, nonetheless, useful insights are provided. For example, with this model the two major trends noted above can be rationalized. First, substitution on the T_d sites by diamagnetic ions for small x will not strongly affect either the intraplanar correlation length or $\langle S^2 \rangle$. J_{inter} will be diminished gradually with increasing x as some of the interlayer connections will be weakened due to the absence of Fe^{3+}, but for layered AF materials J_{inter} need only remain finite in order to generate 3D order. $\langle S^2 \rangle$ will decrease significantly with larger x due to dilution and the rate of decrease of T_c with x will accelerate. J_{inter} will reach a minimum for $x = 1.0$, where all of the Fe^{3+} on the T_d sites has been replaced. Substitution of Mn^{3+} and Cr^{3+} on the O_h sites will generate two effects, an obvious reduction in $\langle S^2 \rangle$ due to the smaller spin quantum numbers and a significant reduction in ξ^2_{2D} as both ions will contribute ferromagnetic intraplanar superexchange interactions according to the Goodenough−Kanamori rules.[27,28] This will of course reduce the size of the AF domains within the planes. Addition of diamagnetic Sc^{3+} at the O_h sites will also reduce $\langle S^2 \rangle$ and ξ^2_{2D} due to dilution but would not introduce competing ferromagnetic correlations. In fact, at the level $x = 0.5$, $\langle S^2 \rangle$ is reduced by a significant fraction relative to Mn^{3+}/Cr^{3+} substitutions but T_c is still higher, indicating an important role for the ferromagnetic intraplanar correlations. Finally, for M = Co substitution of Co^{3+} on both the T_d and the O_h sites will cause the least perturbation to T_c as no ferromagnetic intraplanar correlations will be introduced, again refer to the G−K rules, and the reduction in overall $\langle S^2 \rangle$ will be the main factor which will occur at a lesser rate than for the diamagnetic ion substitutions.

An interesting trend which is perhaps more difficult to understand is the systematic decrease in T_c for the AA′ = CaSr series for the same x as seen in Table 5. For example, this trend does not occur for $Ca_2GaMnO_{5.0}$, $T_c = 160$ K, and $Sr_2GaMnO_{5.0}$, $T_c = 183$ K.[29] It is possible that the modest level of Mn^{3+} which is found on the T_d sites for the AA′ = CaSr series relative to AA′ = Ca_2 contributes to the lowering of T_c due to weakening of J_{inter} through introduction of competing ferromagnetic Fe−O−Mn interactions.

Crystal Structure of AA′ = CaSr, $y \approx 0.5$ Phases, Synthesized in Air. Three members of the CaSr series, x = 0.5, 0.67, and 1.0, were also prepared in air, and the results are summarized for all three in Table 6. As an example, the Rietveld refinement profiles for $x = 0.5$ are shown in Figure 11. Note that all three materials show a cubic perovskite $Pm\bar{3}m$ structure. A Vegard's law correlation, Figure 12, is poorer than that for the argon-synthesized AA′ = Ca_2 series, which may reflect different values of y (Table 6).

Table 6. Summary of Neutron Diffraction Refinement Results at 300 K for $Pm\bar{3}m$ $CaSrFe_{2-x}Mn_xO_{5+y}$ Phases

x	0.50	0.67	1.0
a_0 (Å)	3.8281(1)	3.8219(1)	3.8188(4)
V (Å^3)	56.096(5)	55.824(6)	55.69(2)
R_{wp}	0.0539	0.0603	0.0641
GOF	3.92	1.90	2.20
U_{iso} (Å^2) (Ca/Sr)	0.016(1)	0.0159(8)	0.016(1)
U_{iso} (Å^2) (Fe/Mn)	0.0057(9)	0.0088(8)	0.005(1)
U_{iso} (Å^2) (O)	0.030(1)	0.0305(6)	0.0284(7)
occ. Fe	0.730(3)	0.662(4)	0.495(5)
occ. Mn	0.270(3)	0.338(4)	0.505(5)
occ. O	0.892(3)	0.899(8)	0.92(1)
y (refined)	0.35(2)	0.39(4)	0.50(5)
y (expected)[a]	0.25	0.33	0.50
y (TGA)	0.47(1)	0.53(4)	0.50
Fe(Mn)−O	1.91403(5)	1.91093(6)	1.9094(2)
Ca(Sr)−Ca(Sr)	3.82806(10)	3.82186(13)	3.8188(4)
Ca(Sr)−Fe(Mn)	3.31519(7)	3.30982(8)	3.3072(2)
Ca(Sr)−O	2.70685(5)	2.70246(6)	2.7003(2)

[a]The y value expected assuming that the principal oxidation process is $Mn^{3+} \rightarrow Mn^{4+}$.

Table 6 displays refinement results for the displacement factors and site occupation rates. As for the $y \approx 0$ phases, the Ca/Sr ratio refined to 1.0 to within error. Site occupation rates were refined for the Fe/Mn and O sites. A y value was calculated from the refined O site occupation rate and compared to that expected if all Mn^{3+} is oxidized to Mn^{4+} during synthesis in air. This oxidation mode has been observed for the oxidation of $Sr_2FeMnO_{5.0}$ to $Sr_2FeMnO_{5.5}$. Note first that the Fe/Mn site occupations are in generally good agreement with the nominal Fe/Mn ratios. U_{iso} for the O site is much greater by about a factor of 3 or more than those for the cation sites. In addition, there is reasonable agreement between the derived and the predicted y values from refinement of the O-site occupation; however, the TGA results give somewhat higher values, indicating the possibility of some level of oxidation of Fe^{3+}.

dx.doi.org/10.1021/ja210985t | J. Am. Chem.Soc. 2012, 134, 3215−3227

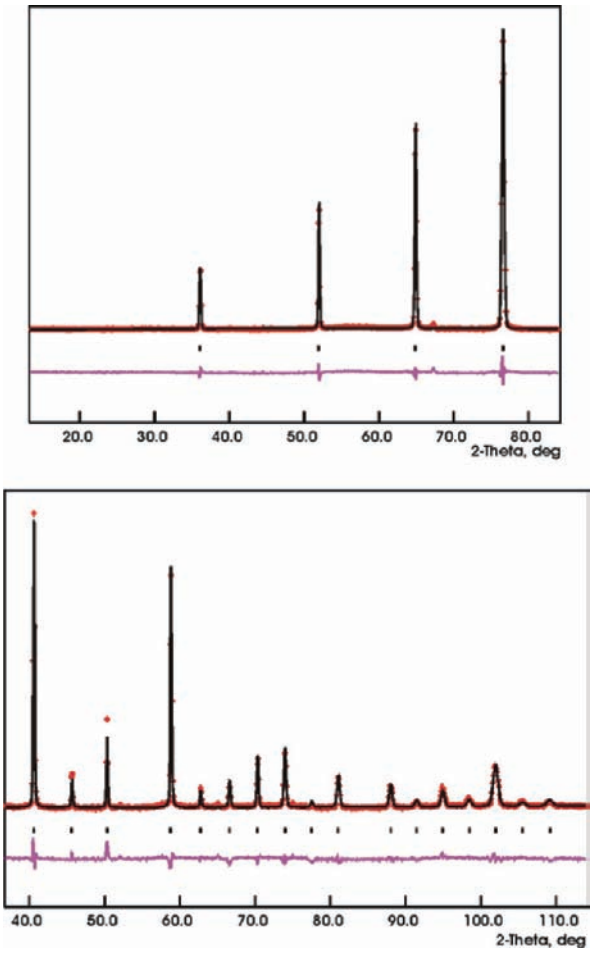

Figure 11. Refinement of neutron diffraction data at 299.6 K for $CaSrFe_{1.5}Mn_{0.5}O_{5+y}$ using wavelengths λ = 2.37242 (top) and 1.33035 Å (bottom) in $Pm\bar{3}m$. See Table 4 for results. Red circles are the data, black line is the fit, lower purple line is the difference, and vertical tic marks locate Bragg Peaks. The very weak unindexed peaks belong to the vanadium container.

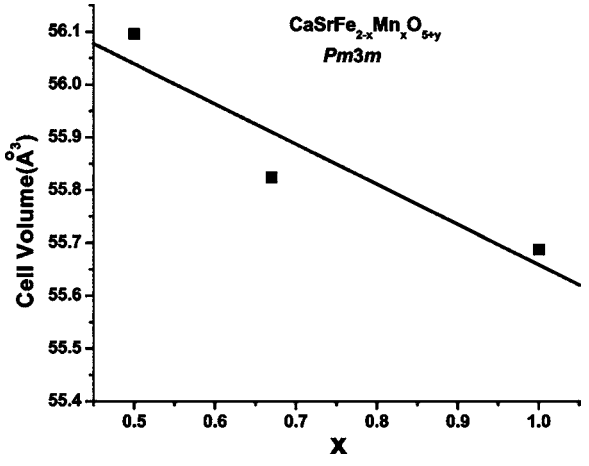

Figure 12. Vegard's law correlation for the cell volume vs x for $CaSrFe_{2-x}Mn_xO_{5+y}$.

Crystal Structure of AA′ = Ca_2 Phases Synthesized in Air. For the purpose of comparison, the Ca_2 phases with x = 0.5 and 0.67 were synthesized. The x = 1 phase has been reported to have a brownmillerite *Pnma* space group.[17] For x = 0.5 and 0.67 cases, formation of a brownmillerite phase was evident from the X-ray powder data, along with a few small peaks indicating the presence of a slight amount of a second phase that could not be identified due to the low intensity of those peaks. These peaks were removed from the X-ray pattern for the final refinements. The absence of the (131) reflection for x = 0.5 and 0.67 indicated that the crystal system is body centered, unlike the argon-synthesized Ca_2 phases with the *Pnma* structure. Figure 13 shows the X-ray refinement profile for the x = 0.5 phase in *Icmm*, and Table 7 lists the refined parameters.

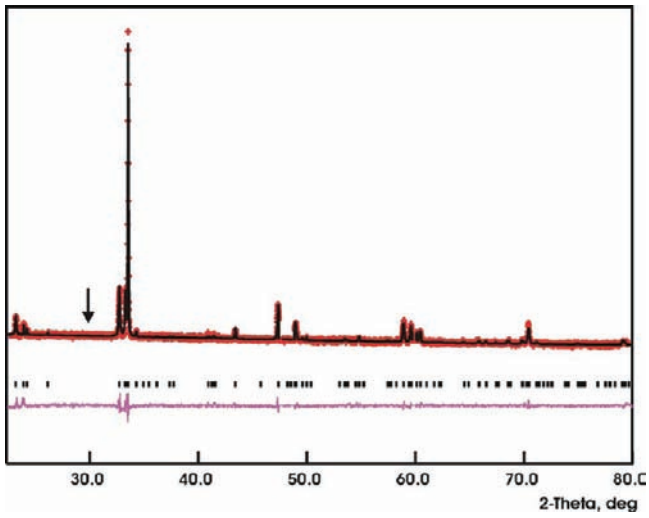

Figure 13. X-ray refinement profile in *Icmm* for $Ca_2Fe_{1.5}Mn_{0.5}O_{5+y}$ synthesized in air. Arrow shows the position where the (131) peak should appear in a *Pnma* system. Its absence in this pattern indicates a body-centered structure.

Table 7. Powder X-ray Refinement Results for $Ca_2Fe_{1.5}Mn_{0.5}O_{5+y}$ Synthesized in Air

	x	y	z	U_{iso}	occ.	site mult.
Ca	0.520(2)	0.6102(4)	0.0	0.025	1	8
Fe1	0.532(2)	0.25	0.433(2)	0.025	0.5	8
Mn1	0.0	0.0	0.0	0.025	0.5	4
Fe2	0.0	0.0	0.0	0.025	0.5	4
O1	0.25	0.996(2)	0.25	0.025	1.0	8
O2	0.004(5)	0.127(1)	0.0	0.025	1.0	8
O3	0.625(9)	0.25	0.198(7)	0.025	0.5	8

space group	*Icmm*
a (Å)	5.47283(29)
b (Å)	14.8948(8)
c (Å)	5.38419(29)

The difference between the Ca_2 and the CaSr phases is remarkable. Synthesis of Ca_2 phases in air or argon always results in the ordering of oxygen vacancies and a brownmillerite structure, even though the degree of oxidation and the oxygen content is considerably higher in the air-synthesized materials, as evident from their unit cell volumes. For example, for the x = 0.5 case, the cell volume is 446.17(5) Å^3 if synthesized in argon and 438.90(7) Å^3 for synthesis in air. On the contrary, the CaSr phases have a brownmillerite structure only when the synthesis is performed in argon. The air-synthesized compounds that

dx.doi.org/10.1021/ja210985t | J. Am. Chem.Soc. 2012, 134, 3215−3227

have higher oxygen contents are cubic perovskites where the oxygen vacancies are disordered.

Local Structure: NPDF. Observation of a high value for U_{iso} at the *O* site, see Table 6, is a common feature for oxygen-deficient perovskites which likely masks a more complex local structure. This was the case for Sr_2FeMnO_5,[12] for example, and many other similar materials which have been investigated using more local probes such as electron diffraction[30,31] or neutron pair distribution function analysis (NPDF). Here, the latter method is applied to one member of the series, $x = 0.5$. Evidence for a complex local structure emerges readily from the $S(Q)$ data shown in Figure 14, which is basically a corrected

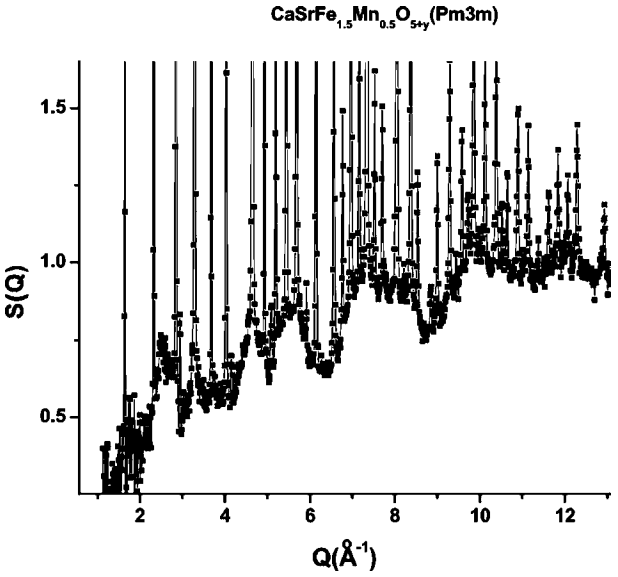

Figure 14. Lower Q portion of the $S(Q)$ for $CaSrFe_{1.5}Mn_{0.5}O_{5+y}$ showing a strongly oscillating background.

and normalized diffraction pattern. Note the oscillating background upon which the $Pm\bar{3}m$ Bragg peaks are superimposed. These oscillations are detectable in the conventional neutron data, but the Q range is more limited. By performing a sine Fourier transform on the $S(Q)$ data the direct space pairwise interatomic distribution function, $G(r)$, is obtained.[32] The intensity of each peak in the $G(r)$ is a product of the neutron scattering lengths of the atoms involved and the number of interatomic interactions at that particular distance. The $G(r)$ data between 1.5 and 4 Å are shown in Figure 15a. The interatomic distances of a cubic model (Table 6) are shown by the dashed vertical lines. It is evident from this figure that the average structure cubic model cannot adequately describe the $G(r)$ data up to 4 Å. There are multiple shoulders and peaks, highlighted by arrows in Figure 15a, that do not match the interatomic interactions of a cubic model. For example, there exists only one Fe(Mn)−O distance at 1.91403(5) Å for a cubic model, while the $G(r)$ contains peaks and shoulders ranging from ∼1.85 to ∼2.45 Å, indicating a more complex local structure. A comparison between the features observed in the $G(r)$ and the interatomic distances of the brownmillerite $CaSrFe_{1.5}Mn_{0.5}O_5$ (Table 4) shows a nice match, suggesting that the local environment of atoms out to 4 Å resembles that of a brownmillerite structure, i.e., local ordering of oxygen vacancies. It is possible to use crystallographic models to fit the $G(r)$ data using the PDFGUI program.[33] A fit out to 4 Å using the average structure model, $Pm\bar{3}m$, shown in Figure 15b, is

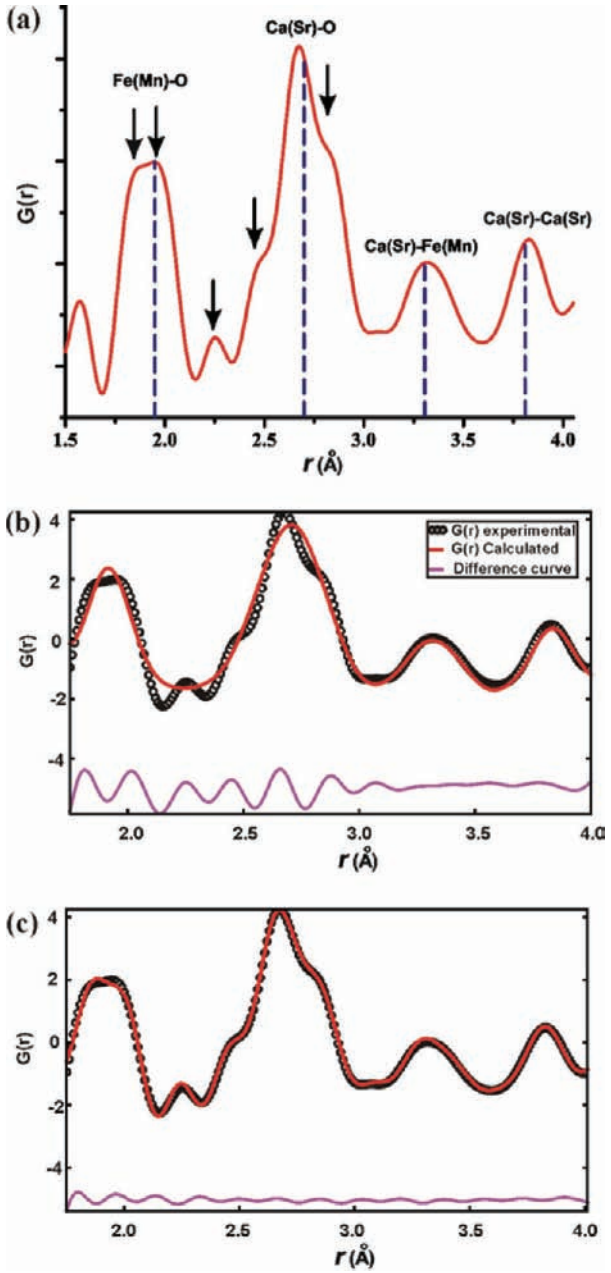

Figure 15. (a) $G(r)$ data for $CaSrFe_{1.5}Mn_{0.5}O_{5+y}$ out to 4 Å. Vertical dashed lines show the interatomic distances of a cubic $Pm\bar{3}m$ model. There are multiple features in the pattern, shown by arrows, that do not match the $Pm\bar{3}m$ model but are in good agreement with a vacancy-ordered, brownmillerite model. (b) $G(r)$ fit using the average structure model, cubic $Pm\bar{3}m$, from 1.76 to 4.00 Å, R_w = 20%, reduced χ^2 = 0.087. As evident from the difference plot, the fit is poor. (c) $G(r)$ fit using a brownmillerite *Ibm*2 model, R_w = 16%, reduced χ^2 = 0.057. The fit is superior, suggesting a local ordering of oxygen vacancies.

poor as expected, while a fit using a brownmillerite *Ibm*2 model gives a good match as seen in Figure 15c. Thus, NPDF analysis suggests a noncubic local structure that resembles the brownmillerite structure with ordering of oxygen vacancies.

Magnetic Properties of $CaSrFe_{2-x}Mn_xO_{5+y}$ Phases Synthesized in Air. No magnetic Bragg peaks were observed in the neutron diffraction patterns at 4 and 300 K, so long-range magnetic order is clearly absent. DC susceptibility data for x = 0.50, 0.67, and 1.0 phases are shown in Figure 16. All three show common features, namely, a distinct ZFC/FC divergence

dx.doi.org/10.1021/ja210985t | J. Am. Chem.Soc. 2012, 134, 3215−3227

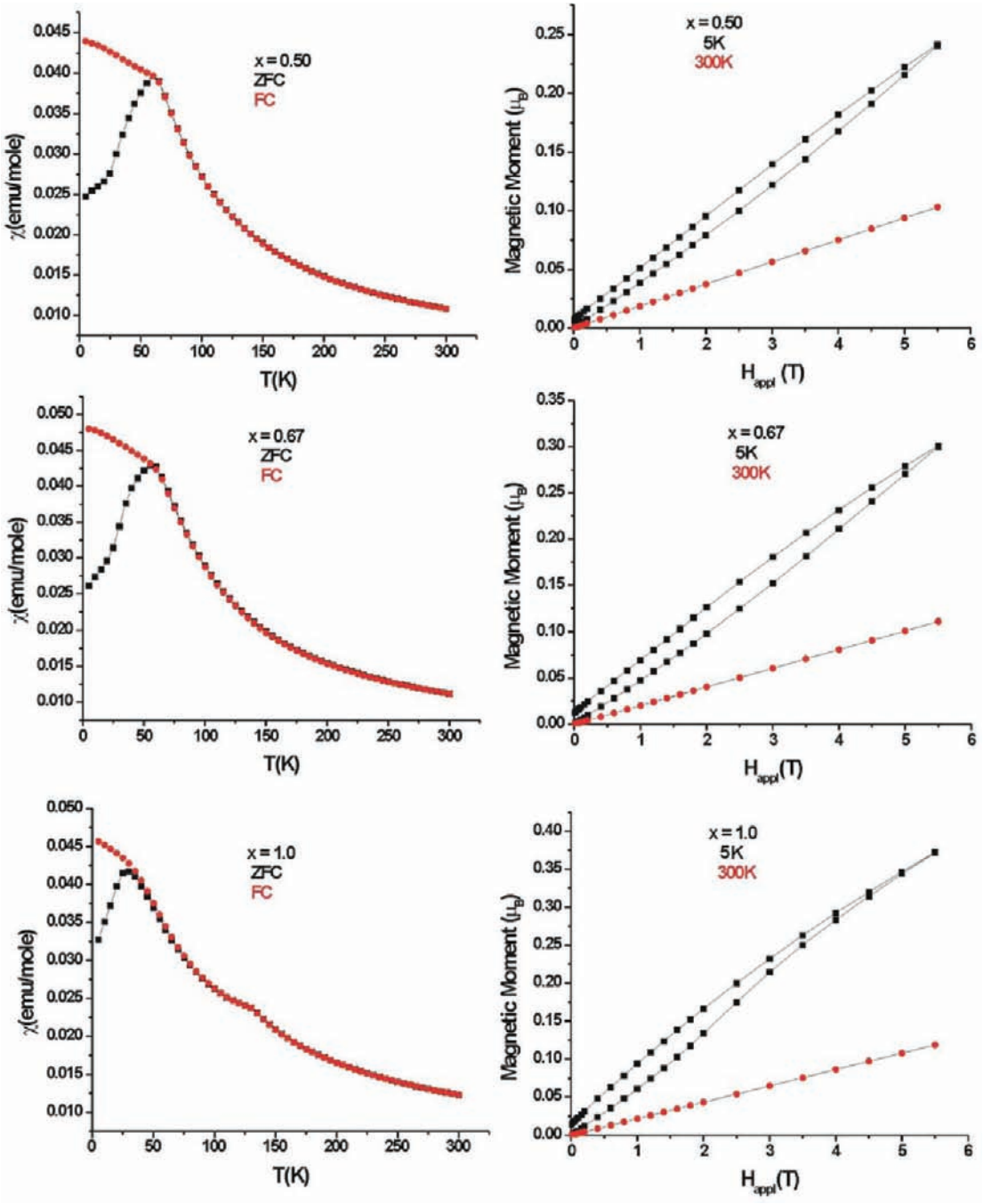

Figure 16. DC susceptibility data for $CaSrFe_{2-x}Mn_xO_{5+y}$: (left) ZFC/FC data; (right) isothermal field sweeps at 300 and 5 K.

at low temperatures near 60 K for x = 0.50 and 0.67 which moves to ~30 K for x = 1.0. Isothermal field sweeps show the development of a weak moment with hysteresis at 5 K for all. Both observations are consistent with some sort of disordered spin ground state but not long-range AF order as found for the $y \approx 0$ vacancy ordered phases. Similar bulk behavior has been reported for $Sr_2FeMnO_{5.0}$ and $Sr_2FeMnO_{5.5}$, but neutron diffraction studies revealed broad magnetic reflections[12] which were commensurate with the average structure unit cell, and a spin glassy ground state was ruled out in favor of superparamagnetism, at least for $Sr_2FeMnO_{5.0}$.

Neutron diffraction data for $CaSrFe_{1.5}Mn_{0.5}O_{5+y}$ were obtained at 4 and 300 K with long acquisition times, and the results are shown in Figure 17a. Note the presence of two very broad features. That centered near ~60° shows no temperature dependence and can be assigned to short-range order of the oxygen vacancies as discussed in the preceding section. It is the first broad oscillation at $Q \approx 2.6$ Å^{-1} in Figure 14. On the other hand, the feature near 31° shows a strong temperature dependence and is magnetic in origin. This reflection was fitted using an Ornstein−Zernike Lorentzian function,[22] as described before $(I(Q) = A/((Q_0 - Q)^2 + \kappa^2)$, and the results are shown in Figure 17b. The fitting parameters are $Q_0 = 1.394(5)$ Å^{-1} which corresponds to $d_0 = 4.51(2)$ Å and $\kappa = 0.15(1)$ Å^{-1} which corresponds to a correlation length, $\xi = 6.7(4)$ Å. The derived d_0 is not commensurate with any simple multiple of the

dx.doi.org/10.1021/ja210985t | J. Am. Chem.Soc. 2012, 134, 3215−3227

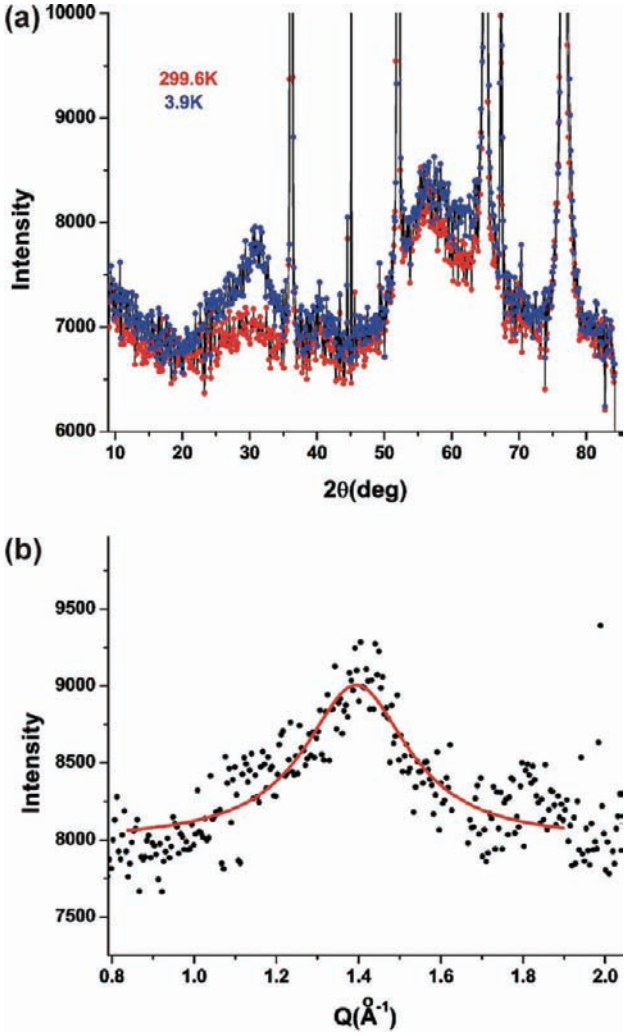

Figure 17. (a) Neutron diffraction data at 3.9 and 299.6 K for $CaSrFe_{1.5}Mn_{0.5}O_{5+y}$ synthesized in air. (b) Fit of the magnetic reflection at 3.9 K in $CaSrFe_{1.5}Mn_{0.5}O_{5+y}$ (synthesized in air) to a Lorentzian as described in the text.

average cubic cell which is distinctly different from the case of $Sr_2FeMnO_{5.0}$ where two reflections could be indexed on a doubled cubic cell.[12] However, Q_0 does lie near the positions for the strongest magnetic Bragg peaks for the corresponding ordered brownmillerite $x = 0.5$ phase, $Q = 1.392$ and 1.418 Å^{-1}, which is consistent with the NPDF results that suggested a brownmillerite local structure. The correlation length is slightly greater than next-nearest-neighbor distances but slightly shorter than the interlayer spacing. Given the short correlation length, perhaps a spin frozen ground state model is more relevant in this case.

SUMMARY AND CONCLUSIONS

The effects of varying the composition by substitution on both the AA′ and the BB′ sites as well as the effect of oxygen stoichiometry in oxygen-deficient perovskites of the type $AA'B-B'O_{5+y}$ have been investigated systematically for the two series $Ca_2Fe_{2-x}Mn_xO_{5+y}$ and $CaSrFe_{2-x}Mn_xO_{5+y}$ for $x = 0.50$, 0.67, and 1.0 and $y \approx 0$ and 0.3−0.5. For the same x and $y \approx 0$ the change in A-site composition has two principal effects. First, the space group changes from *Pnma* (Ca_2) to *Icmm* (CaSr) and the tendency for Mn^{3+} to occupy the O_h sites is slightly diminished. The former observation appears to be somewhat at odds with the structure-field map proposed by Parsons et al.[15] In this scheme, the expected sequence upon increasing the separation between T_d chain layers is *Pnma*−*Ibm*2−*Icmm*. The refinements done in the present study on the CaSr phases show better agreement indices for *Icmm* than for *Ibm*2. However, tests for a polar space group were not done, so the force of this observation should be tempered somewhat. Certainly, the most remarkable result concerns $CaSrFeMnO_{5.0}$. Here, for samples prepared in argon, brownmillerite vacancy ordering persists but only on a short-range length scale ∼160 Å. This situation represents an intermediate case in the sequence $Ca_2FeMnO_{5.0}$(*Pnma*)−$CaSrFeMnO_5$ (*Icmm*, short-range)−$Sr_2FeMnO_{5.0}$ ($Pm\bar{3}m$), which reflects increasingly disordered T_d chains as the average A site radius is increased systematically.

For the same AA′, increasing x (Mn^{3+} content) decreases the unit cell volume with a Vegard's law linearity. This is somewhat surprising as the accepted radii for Mn^{3+} and Fe^{3+}, both high spin and with CN = 6, are identical, 0.645 Å.[34] Nonetheless, in these materials Mn^{3+} appears to be smaller.

The effect of these substitutions on the magnetic properties is also remarkable. For $Ca_2Fe_{2-x}Mn_xO_{5.0}$ increasing the Mn content, up to $x = 0.50$, decreases T_c to a much greater extent than that seen for simple dilution by diamagnetic ions for the same x. This is discussed in terms of a layered AF model and is attributed to introduction of ferromagnetic Fe−O−Mn superexchange interactions mainly within the O_h layers. These ideas are extended to provide a qualitative rationalization of the known T_c values for several $Ca_2Fe_{2-x}M_xO_5$ materials. For $x = 0.50$ in both series there is a cross over from a G_y to a G_x magnetic anisotropy with increasing temperature which appears to be consistent with the previously known magnetic anisotropies of brownmillerite oxides.

Finally, regarding the materials prepared in air, $y > 0$, the vacancy ordering is preserved in $Ca_2Fe_{2-x}Mn_xO_{5+y}$ series, although a change from *Pnma* to *Icmm* symmetry is observed when these phases are prepared in air for $x = 0.5$ and 0.67. However, for the $CaSrFe_{2-x}Mn_xO_{5+y}$ series, $y > 0$, the long-range brownmillerite vacancy ordering is destroyed and a cubic $Pm\bar{3}m$ symmetry is found for all x. Refined values for y from neutron diffraction data are in reasonable agreement with those expected if the main oxidation mechanism involves conversion of Mn^{3+} to Mn^{4+}. An NPDF study of the local structure of the $x = 0.50$ phase shows that on very short length scales up to 4 Å a brownmillerite-type model provides a better fit to the data than the average $Pm\bar{3}m$ structure.

Also, for the $y > 0$ CaSr series members, long-range magnetic G-type AF order found for the $y \approx 0$ phases is destroyed and bulk susceptibility features typical of spin frozen ground states are observed. For $x = 0.50$ neutron diffraction data disclose a diffuse magnetic peak, incommensurate with the average cubic cell. The very short correlation length of ∼7 Å is not inconsistent with a frozen spin ground state.

AUTHOR INFORMATION

Corresponding Author
greedan@mcmaster.ca

ACKNOWLEDGMENTS

J.E.G. acknowledges the support of the Natural Sciences and Engineering Research Council (NSERC) of Canada through Discovery Grants. The authors thank Frank Gibbs for his help

with the TGA measurements. This work has benefited from the use of NPDF at the Lujan Center at Los Alamos Neutron Science Center, funded by the DOE Office of Basic Energy Sciences. Los Alamos National Laboratory is operated by Los Alamos National Security LLC under DOE Contract DE-AC52-06NA25396. The upgrade of NPDF has been funded by the NSF through grant DMR 00-76488. The Canadian Neutron Beam Centre is funded jointly by NSERC and the National Research Council (NRC) of Canada. The work at the High Flux Isotope Reactor, Oak Ridge National Laboratory (ORNL), was sponsored by the Scientific User Facilities Division, Office of Basic Energy Sciences, U.S. Department of Energy (U.S. DOE). ORNL is operated by UT Battelle, LLC for the U.S. DOE under Contract No. DEAC05-00OR22725.

REFERENCES

(1) Chan, T. S.; Liu, R. S.; Yang, C. C.; Li, W. -.; Lien, Y. H.; Huang, C. Y.; Lynn, J. W. *J. Magn. Magn. Mater.* **2007**, *310*, 1151−1153.
(2) Sheptyakov, D. V.; Abakumov, A. M.; Antipov, E. V.; Balagurov, A. M.; Billinge, S. J. L.; Fischer, P.; Keller, L.; Lobanov, M. V.; Pavlyuk, B. P.; Pomjakushin, V. Y.; Rozova, M. G. *Appl. Phys. A: Mater. Sci. Process.* **2002**, *74* (Suppl.), S1734−S1736.
(3) Wright, A. J.; Palmer, H. M.; Anderson, P. A.; Greaves, C. *J. Mater. Chem.* **2002**, *12*, 978−982.
(4) Diethelm, S.; Van herle, J. *J. Eur. Ceram. Soc.* **2004**, *24*, 1319−1323.
(5) Hu, J.; Hao, H.; Chen, C.; Yang, D.; Hu, X. *J. Membr. Sci.* **2006**, *280*, 809−814.
(6) Wang, B.; Zhan, M.-c.; Zhu, D.-c.; Liu, W.; Chen, C.-s. *J. Solid State Electrochem.* **2006**, *10*, 625−628.
(7) Ramezanipour, F.; Cowie, B.; Derakhshan, S.; Greedan, J. E.; Cranswick, L. M. D. *J. Solid State Chem.* **2009**, *182*, 153−159.
(8) Berggren, J. *Acta Chem. Scand.* **1971**, *25*, 3616−3624.
(9) Takeda, T.; Yamaguchi, Y.; Tomiyoshi, S.; Fukase, M.; Sugimoto, M.; Watanabe, H. *J. Phys. Soc. Jpn.* **1968**, *24*, 446−452.
(10) Schmidt, M.; Campbell, S. J. *J. Solid State Chem.* **2001**, *156*, 292−304.
(11) Hodges, J. P.; Short, S.; Jorgensen, J. D.; Xiong, X.; Dabrowski, B.; Mini, S. M.; Kimball, C. W. *J. Solid State Chem.* **2000**, *151*, 190−209.
(12) Ramezanipour, F.; Greedan, J. E.; Siewenie, J.; Proffen, T.; Ryan, D. H.; Grosvenor, A. P.; Donaberger, R. L. *Inorg. Chem.* **2011**, *50*, 7779−7791.
(13) Battle, P. D.; Bollen, S. K.; Gibb, T. C.; Matsuo, M. *J. Solid State Chem.* **1991**, *90*, 42−46.
(14) Gibb, T. C.; Matsuo, M. *J. Solid State Chem.* **1990**, *86*, 164−174.
(15) Parsons, T. G.; D'Hondt, H.; Hadermann, J.; Hayward, M. A. *Chem. Mater.* **2009**, *21*, 5527−5538.
(16) Ramezanipour, F.; Greedan, J. E.; Grosvenor, A. P.; Britten, J. F.; Cranswick, L. M. D.; Garlea, V. O. *Chem. Mater.* **2010**, *22*, 6008−6020.
(17) Nakahara, Y.; Kato, S.; Sugai, M.; Ohshima, Y.; Makino, K. *Mater. Lett.* **1997**, *30*, 163−167.
(18) Geller, S.; Grant, R. W.; Gonser, U.; Wiedersich, H.; Espinosa, G. P. *Phys. Lett. A* **1967**, *25*, 722.
(19) Grant, R. W.; Wiedersich, H.; Geller, S.; Gonser, U.; Espinosa, G. P. *J. Appl. Phys.* **1967**, *38*, 1455−1456.
(20) Grenier, J.-C.; Pouchard, M.; Hagenmuller, P. *J. Solid State Chem.* **1975**, *13*, 92−98.
(21) Proffen, T.; Egami, T.; Billinge, S. J. L.; Cheetham, A. K.; Louca, D.; Parise, J. B. *Appl. Phys. A: Mater. Sci. Process.* **2002**, *74*, s163−s165.
(22) Stanley, H. E. In *Introduction to Phase Transitions and Critical Phenomena*; Oxford Univ. Press: New York, 1971.
(23) Collins, M. F. In *Magnetic Critical Scattering*; Oxford University Press: New York, Oxford, 1989; p 29.
(24) Geller, S.; Grant, R. W.; Gonser, U. *Prog. Solid State Chem.* **1971**, *5*, 1−26.
(25) Gibb, T. C.; Matsuo, M. *J. Solid State Chem.* **1990**, *88*, 485−497.
(26) de Jongh, L. J. In *Magnetic Properties of Layered Transition Metal Compounds*; Kluwer Academic Publishers: Dordrecht, 1990; p 19.
(27) Goodenoug, J. B. In *Magnetism and the Chemical Bond*; Interscience: New York, London, 1963; pp 174−178.
(28) Kanamori, J. *J. Phys. Chem. Solids* **1959**, *10*, 87.
(29) Pomjakushin, V. Y.; Balagurov, A. M.; Elzhov, T. V.; Sheptyakov, D. V.; Fischer, P.; Khomskii, D. I.; Yushankhai, V. Y.; Abakumov, A. M.; Rozova, M. G.; Antipov, E. V.; Lobanov, M. V.; Billinge, S. J. L. *Phys. Rev. B* **2002**, *66*, 184412.
(30) Vallet-Regi, M.; Gonzalez-Calbet, J. M.; Verde, J.; Alario-Franco, M. A. *J. Solid State Chem.* **1985**, *57*, 197−206.
(31) González-Calbet, J. M.; Alonso, J.; Vallet-Regí, M. *J. Solid State Chem.* **1987**, *71*, 331−341.
(32) Billinge, S. J. L.; Kanatzidis, M. G. *Chem. Commun.* **2004**, 749−760.
(33) Farrow, C. L.; Juhás, P.; Liu, J. W.; Bryndin, D.; Božin, E. S.; Bloch, J.; Proffen, T.; Billinge, S. J. L. *J. Phys.: Condens. Matter* **2007**, *19*, 335219.
(34) Shannon, R. D. *Acta Crystallogr.* **1976**, *A32*, 751−767.